

## **Supporting Information**

### **Zinc removal from aqueous solution using a deionization pseudocapacitor with a high-performance nanostructured birnessite electrode**

Lihu Liu,<sup>a</sup> Yao Luo,<sup>a</sup> Wenfeng Tan,<sup>a</sup> Fan Liu,<sup>a</sup> Steven L. Suib,<sup>b</sup> Yashan Zhang<sup>b</sup> and Guohong Qiu<sup>\*a</sup>

<sup>a</sup>Key Laboratory of Arable Land Conservation (Middle and Lower Reaches of Yangtse River), Ministry of Agriculture, College of Resources and Environment, Huazhong Agricultural University, Wuhan 430070, China

<sup>b</sup> Department of Chemistry, University of Connecticut, Storrs, 55 North Eagleville Road, Storrs, Connecticut, 06269-3060, United States

\* Corresponding author: Qiu GH, qiugh@mail.hzau.edu.cn

**SI Supporting material and methods**

**SII Supporting tables and figures**

**24 Pages, 2 Tables and 16 Figures**

## **SI Supporting material and methods**

### **S1. Synthesis of hetaerolite and Zn-birnessite**

The hetaerolite was prepared by a solvothermal method.<sup>1</sup> 4.0 mmol  $\text{Mn}(\text{NO}_3)_2$ , 2.0 mmol  $\text{Zn}(\text{NO}_3)_2 \cdot 7\text{H}_2\text{O}$ , 0.25 mmol cetyltrimethylammonium bromide (CTAB), and 2.0 mmol citric acid were mixed and dissolved into 60 mL anhydrous ethanol. The mixture was then stirred for 3 h and subsequently transferred in an 80 mL Teflon-lined stainless-steel autoclave, and solvothermally treated at 160 °C for 48 h. The resulting precipitate was filtered and washed with DDW and subsequently ethanol until the filtrate conductivity was below 20.0  $\mu\text{S cm}^{-1}$ . Then, the as-prepared product was dried in an oven at 60 °C for 24 h.

The Zn-birnessite was prepared by an ion-exchange method.<sup>2</sup> 250 mL NaOH (6.0 mol  $\text{L}^{-1}$ ) solution was poured into 200 mL (0.5 mol  $\text{L}^{-1}$ )  $\text{MnCl}_2$  solution with vigorous stirring at temperature of 5 °C, and then  $\text{O}_2$  was bubbled at a rate of 2.0  $\text{L min}^{-1}$ . After 30 min, the resulting precipitate was filtered and washed with DDW until the filtrate conductivity was below 20.0  $\mu\text{S cm}^{-1}$ , and the moist solid was characterized to be Na-buserite. Zn-buserite was prepared through shaking the mixture of 10.0 g moist Na-buserite and 500 mL  $\text{ZnSO}_4$  solution of 1.0 mol  $\text{L}^{-1}$  at room temperature for 12 h. Excess salt was removed by DDW and moist Zn-birnessite was obtained. Zn-birnessite powder was obtained by dehydration of the Zn-buserite at 60 °C for 24 h.

### **S2. Preparations of birnessite electrodes and Zn-containing wastewater**

The electrochemical tests were performed with a three-electrode system at room temperature. The working electrode was fabricated by coating a mixture of electro-active material (birnessite), conductive acetylene black, and polymeric binder polyvinylidene fluoride (PVDF) with a mass ratio of 75: 15: 10 on carbon fabric with the dimension of 1.5 cm  $\times$  2.5 cm (Shanghai Hesens Electric Co.

Ltd.). Another pure carbon fabric and a saturated calomel electrode (SCE) were used as counter and reference electrodes, respectively.

Zn-containing wastewater was prepared by  $\text{ZnSO}_4$  solution and the initial pH value was controlled at 5.5 with  $\text{H}_2\text{SO}_4$  ( $0.1 \text{ mol L}^{-1}$ ) and  $\text{NaOH}$  ( $0.1 \text{ mol L}^{-1}$ ). The  $\text{Zn}^{2+}$  removal capacity was evaluated with initial  $\text{Zn}^{2+}$  concentrations of 0, 200, 600, 1000, 1400, and 1800  $\text{mg L}^{-1}$ , respectively. The influence of initial pH value on the  $\text{Zn}^{2+}$  removal capacity was studied at 3.5, 4.0, 4.5, 5.0, and 5.5 with  $\text{Zn}^{2+}$  initial concentration of 200  $\text{mg L}^{-1}$ . The effect of birnessite mass on  $\text{Zn}^{2+}$  removal was further investigated in electrolyte containing 200  $\text{mg L}^{-1}$   $\text{Zn}^{2+}$  with an initial pH of 5.5, and the mass of birnessite was respectively controlled at 0, 3.75, 7.50, 11.25, and 15.00 mg. All supporting electrolytes in the above solutions were  $0.1 \text{ mol L}^{-1}$   $\text{Na}_2\text{SO}_4$ .

### **S3. Isothermal adsorption of $\text{Zn}^{2+}$ by birnessite**

The isothermal adsorption of  $\text{Zn}^{2+}$  on the as-obtained birnessite was conducted, and the results were compared with those of the electrochemical removal. A birnessite suspension of  $5.0 \text{ g L}^{-1}$  was prepared with  $0.1 \text{ mol L}^{-1}$   $\text{Na}_2\text{SO}_4$ , and the pH value of the suspension was previously adjusted and maintained at 5.5 for 24 h using  $0.1 \text{ mol L}^{-1}$   $\text{H}_2\text{SO}_4$  and  $0.1 \text{ mol L}^{-1}$   $\text{NaOH}$ . A 15-mL birnessite suspension of  $1.67 \text{ g L}^{-1}$  was used for adsorption experiment with initial concentrations of  $\text{Zn}^{2+}$  ranging from 0 to 650  $\text{mg L}^{-1}$ . The ionic strength was controlled using  $0.1 \text{ mol L}^{-1}$   $\text{Na}_2\text{SO}_4$ . The resulting suspensions were shaken with a speed of  $200 \text{ rpm min}^{-1}$  at  $25 \text{ }^\circ\text{C}$  for 24 h, and the pH value was controlled at  $5.50 \pm 0.05$  during the equilibration period. The concentration of  $\text{Zn}^{2+}$  in solution was determined by atomic absorption spectroscopy after centrifugal separation, and the moist solid was characterized by XRD. Each experiment was performed in triplicate.

#### S4. Spectroscopic analyses of samples and birnessite electrodes

The crystal structure of the as-prepared hetaerolite was characterized by X-ray diffractometer (XRD, Bruker D8 ADVANCE, Cu K $\alpha$ ,  $\lambda = 0.15406$  nm) using an operation voltage and current of 40 kV and 40 mA at a scanning rate of  $10^\circ \text{ min}^{-1}$  and a step size of  $0.02^\circ$ .

The Mn AOS and transformation products of birnessite in the charge–discharge processes were also analyzed by the XAFS spectra. Mn K-edge XAFS data were collected in transmission mode over the energy range of 6340–7327 eV. The ion-chamber detector was filled with 100% N<sub>2</sub>. The monochromator energy was calibrated to the first derivative of Mn metal foil ( $E_0 = 6539$  eV). XAFS spectra were processed using the program Ifeffit/Athena.<sup>3</sup> Parameters ( $E_0 = 6548$  eV, Rbkg =  $1.0 \text{ \AA}$ , and k-weight = 2) were used for background removal of Mn K-edge spectra. Zn K-edge XAFS data were collected in transmission mode over the energy range of 9462–10366 eV. The ion-chamber detector filled with 17% Ar. The monochromator energy was calibrated to the first derivative of Zn metal foil ( $E_0 = 9659$  eV). Parameters ( $E_0 = 9665$  eV, Rbkg =  $1.0 \text{ \AA}$ , and k-weight = 2) were used for background removal of Zn K-edge spectra.

#### S5. Calculation of electrochemical specific capacitance and Zn<sup>2+</sup> removal capacity

The electrochemical specific capacitance and the Zn<sup>2+</sup> removal capacity were respectively calculated according to [Equation S1](#) and [Equation S2](#):

$$C_m = \frac{I\Delta t}{m\Delta V} \quad (\text{S1})$$

$$Q_s = \frac{(C_0 - C_s)V_s}{m} \quad (\text{S2})$$

In these equations,  $C_m$  (F g<sup>-1</sup>) is the electrochemical specific capacitance,  $I$  (A) is the current density,  $\Delta t$  (s) is the discharge time,  $m$  (g) is the

mass of birnessite on the working electrode, and  $\Delta V$  (V) is the potential window,  $Q_s$  ( $\text{mg g}^{-1}$ ) is the  $\text{Zn}^{2+}$  removal capacity,  $C_0$  ( $\text{mg L}^{-1}$ ) is the initial concentration of  $\text{Zn}^{2+}$  in the reaction system,  $C_s$  ( $\text{mg L}^{-1}$ ) is the concentration of  $\text{Zn}^{2+}$  in the solution after galvanostatic charge–discharge tests, and  $V_s$  (L) is the volume of solution.

## SII Supporting tables and figures

**Table S1** Fractional and average valence states of Mn obtained from the Combo fit of Mn K-edge XANES spectra of HB and HB electrodes after 50 cycles of charge–discharge tests in electrolytes with different  $Zn^{2+}$  concentrations in the 6521–6653 eV interval.

References (code name)	HB	HB-0	HB-200	HB-600	HB-1000
Pyrolusite (REF4-1)	–	–	–	–	0.11
Ramsdellite (REF4-2)	0.17	0.24	0.20	0.18	0.07
Ca <sub>2</sub> Mn <sub>3</sub> O <sub>8</sub> (REF4-3)	0.13	0.20	0.24	0.17	0.10
KBi (REF4-4)	0.44	0.32	0.30	0.29	0.24
Groutite (REF3-1)	0.11	0.12	0.14	0.02	
Feitknechtite (REF3-2)	–	–	–	0.17	0.12
Manganite (REF3-3)	–	–	–	0.10	0.33
Mn <sub>2</sub> O <sub>3</sub> (REF3-4)	–	–	–	–	–
MnPO <sub>4</sub> (REF3-5)	0.05	0.01	0.02	0.02	
Hureaulite (REF2-1)	–	–	–	–	–
Fungi (REF2-2)	0.06	–	0.01	–	–
Rhodocrosite (REF2-3)	0.03	0.01	–	–	–
Manganosite (REF2-4)	–	–	–	–	–
Pyroxmangite (REF2-5)	–	0.04	0.04	0.05	0.03
Tephroite (REF2-6)	–	–	–	–	–
MnSO <sub>4</sub> (aq) (REF2-7)	0.01	0.06	0.05	–	–
MnSO <sub>4</sub> (s) (REF2-8)	–	–	–	–	–
$NSS \times 10^5$	3.53	2.74	3.24	4.06	8.40
Sum of Mn <sup>2+</sup> (at.%)	0.10	0.11	0.10	0.05	0.03
Sum of Mn <sup>3+</sup> (at.%)	0.16	0.13	0.16	0.31	0.45
Sum of Mn <sup>4+</sup> (at.%)	0.74	0.76	0.74	0.64	0.52
Mn AOS	3.64	3.65	3.64	3.59	3.49

$NSS$  is the normalized sum-squared residual =  $\sum_n[\text{data} - \text{fit}]^2 / \sum_n[\text{data}]^2$ .

Due to the large variability in chemical compositions and crystal structures of mixed-valent manganates, a large series of XANES spectra of standard Mn compounds with single valence state of Mn, known chemical composition and

structures are used for linear combinations of pure Mn species in the Combo method.<sup>4</sup> This method differs from the usual linear combination fitting. Regardless of the chemical and polyhedral similarity between the references and the unknown samples, all of the seventeen references are included in the linear combination fitting. The relative contents of  $\text{Mn}^{2+}$ ,  $\text{Mn}^{3+}$ , and  $\text{Mn}^{4+}$  in unknown samples are taken as the sum of all positive fractions for the references of  $\text{Mn}^{2+}$ ,  $\text{Mn}^{3+}$ , and  $\text{Mn}^{4+}$ , respectively.<sup>4</sup> The Combo method can not indicate whether the unknown samples are similar to the references in structure or are the mixtures of the references. What makes sense is the grouping of all components belonging to the same oxidation state.<sup>4</sup>

**Table S2** Relative contents of birnessite, Zn-buserite, and  $\text{ZnMn}_2\text{O}_4$  obtained from the fitting results of Mn K-edge EXAFS spectra in HB electrodes after 50 cycles of charge–discharge tests in electrolytes with different  $\text{Zn}^{2+}$  concentrations.

Electrodes	Birnessite (%)	Zn-birnessite (%)	$\text{ZnMn}_2\text{O}_4$ (%)	$\chi_{\text{red}}^2$	R-factor
HB-200	94	0	6	0.1	0.007
HB-600	81	3	16	0.1	0.009
HB-1000	61	9	30	0.3	0.028

The R-factor increased with the increase of  $\text{Zn}^{2+}$  concentration in electrolyte, which was likely due to the difference in chemical composition between Zn-birnessite on the electrodes and Zn-birnessite synthesized by ion-exchange method. This was also possibly due to the formation or adsorption of some new materials when  $\text{Zn}^{2+}$  concentration was increased to 600 and 1000  $\text{mg L}^{-1}$ . The Mn K-edge  $k^3$ -weighted EXAFS spectra of birnessite electrodes could not be very well fitted possibly due to the complicated electrochemical adsorption and transformation processes.

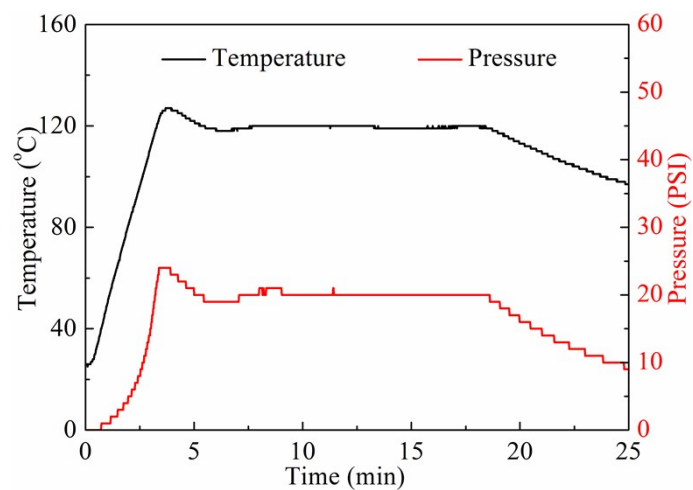


**Fig. S1** Temperature and pressure curves of the hydrothermal reaction of  $\text{KMnO}_4$  and  $\beta$ -cyclodextrin under microwave irradiation.

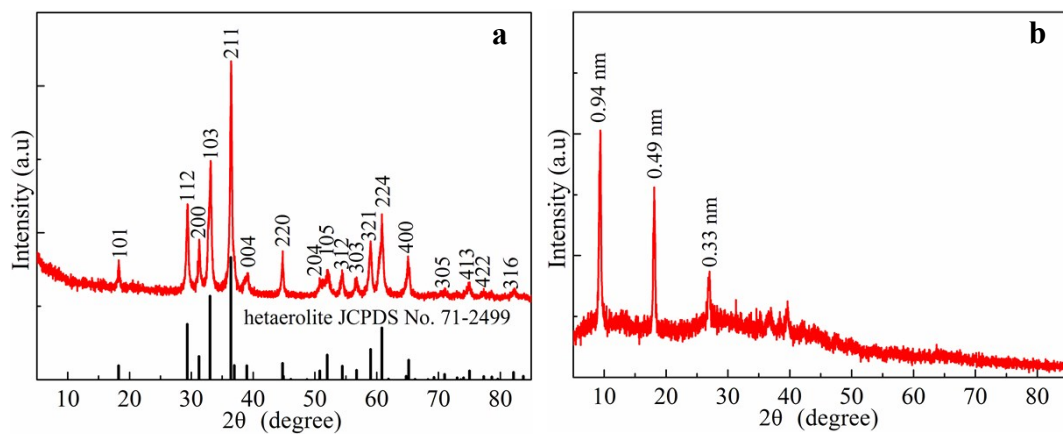


**Fig. S2** XRD patterns of as-obtained hetaerolite (a) and wet Zn-buserite (b).

As shown in Fig. S2a, all the diffraction peaks in XRD patterns for the sample were indexed to hetaerolite (JCPDS card no. 71-2499). The XRD peaks of wet Zn-buserite (Fig. S2b) was consistent with the previous report.<sup>2</sup>

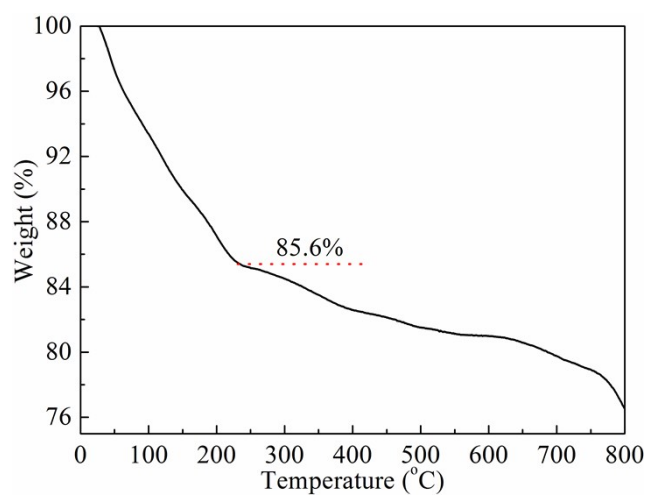


**Fig. S3** TGA curve of synthesized birnessite obtained at a heating rate of  $10\text{ }^{\circ}\text{C min}^{-1}$  in nitrogen atmosphere.

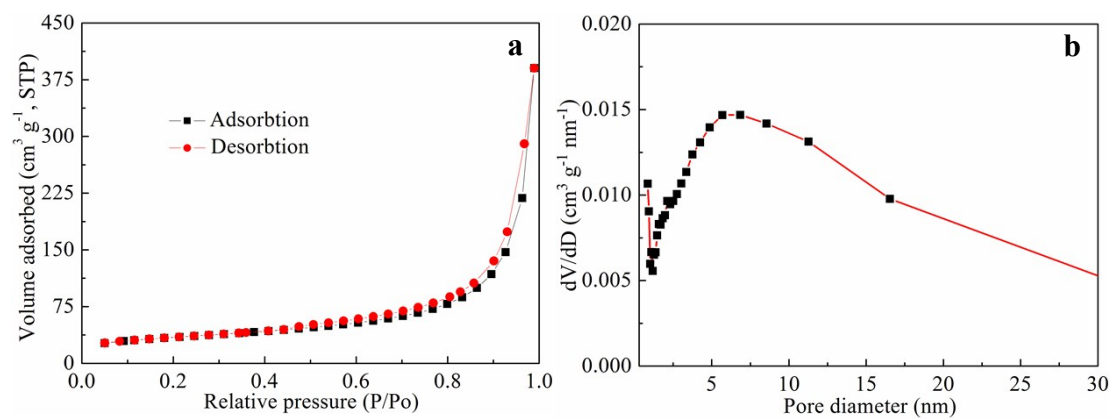


**Fig. S4**  $N_2$  adsorption–desorption isotherms (a) and pore size distribution (b) of synthesized birnessite.

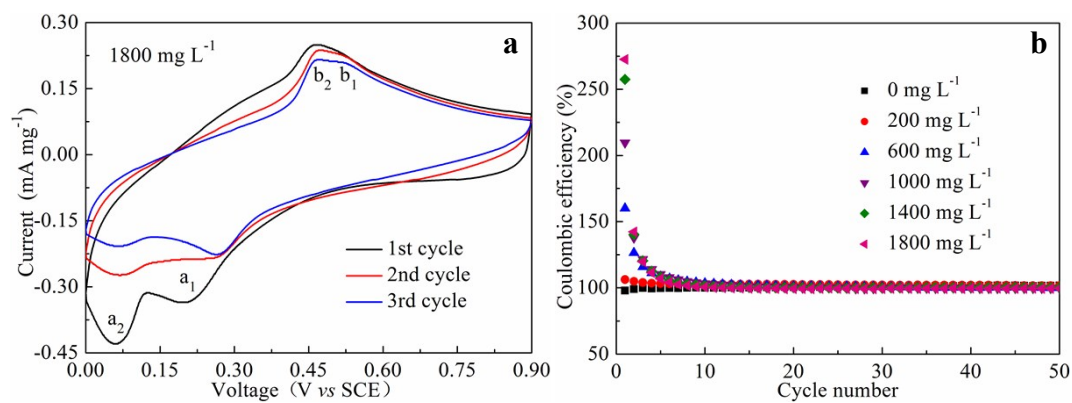


**Fig. S5** Cyclic voltammety curves for the first three cycles of birnessite electrode in  $1800 \text{ mg L}^{-1}$   $\text{Zn}^{2+}$  electrolyte at a scan rate of  $0.5 \text{ mV s}^{-1}$  (a) and coulombic efficiency of birnessite electrodes at a current density of  $0.1 \text{ A g}^{-1}$  in  $\text{Na}_2\text{SO}_4$  electrolytes with different  $\text{Zn}^{2+}$  concentrations (b).

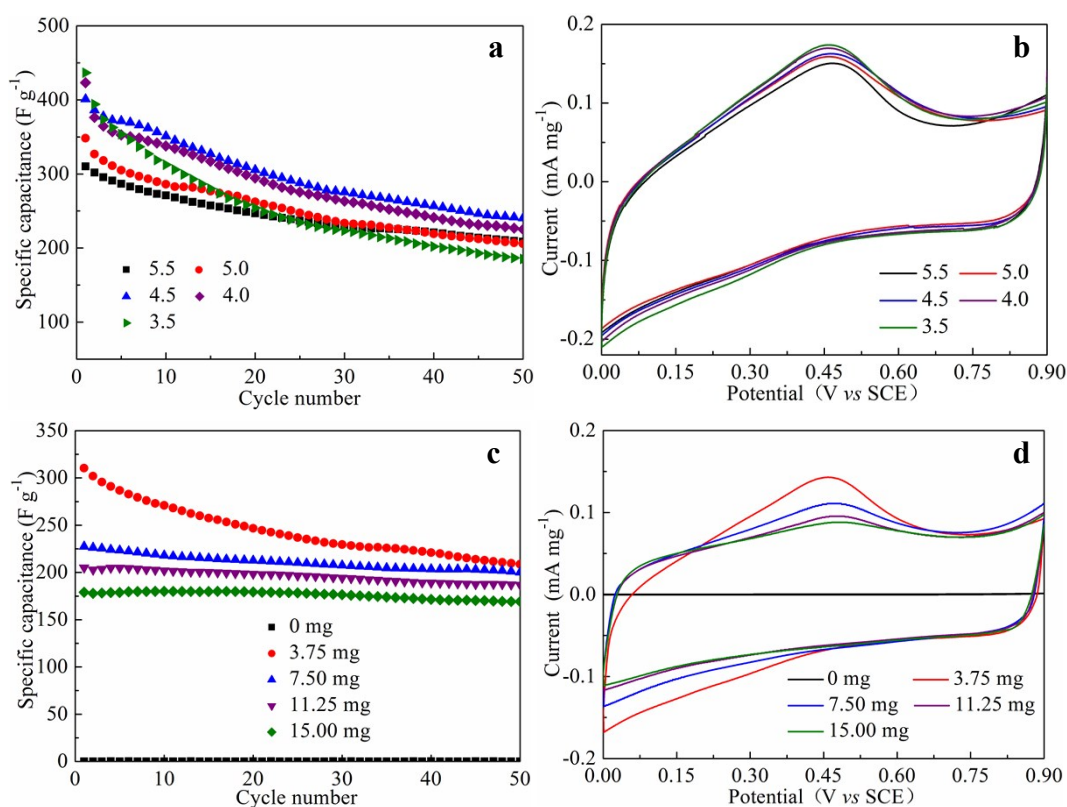


**Fig. S6** Cyclic capacitance at a current density of 0.1 A g<sup>-1</sup> and cyclic voltammetry curves for the first cycle at a scan rate of 0.5 mV s<sup>-1</sup> of birnessite electrodes (a, b) and that of different masses of active birnessite electrode (c, d) in 200 mg L<sup>-1</sup> Zn<sup>2+</sup> electrolyte.

As seen from Fig. S6a, the initial electrochemical specific capacitance of birnessite increased with decreasing initial pH in the electrolyte. However, low pH led to the rapid decay of electrochemical specific capacitance during the charge–discharge process. This change trend was further confirmed by cyclic voltammetry test (Fig. S6b). As seen in Fig. S6c, the electrochemical specific capacitance of carbon fabric, acetylene black, and PVDF was negligible, indicating that no Zn<sup>2+</sup> was adsorbed on the carbon fabric and PVDF. The initial electrochemical specific capacitance decreased with the increase of birnessite mass, which was in good agreement with the result of cyclic voltammetry test (Fig. S6d). During charge–discharge tests, the decay of electrochemical specific capacitance became less dramatic with an increase in the mass of birnessite.

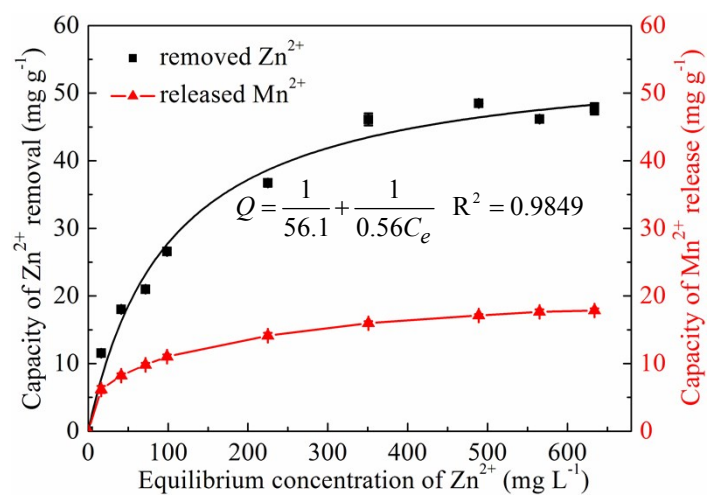


**Fig. S7** Isotherm of  $\text{Zn}^{2+}$  adsorption on the synthesized birnessite and  $\text{Mn}^{2+}$  release with pH 5.5.

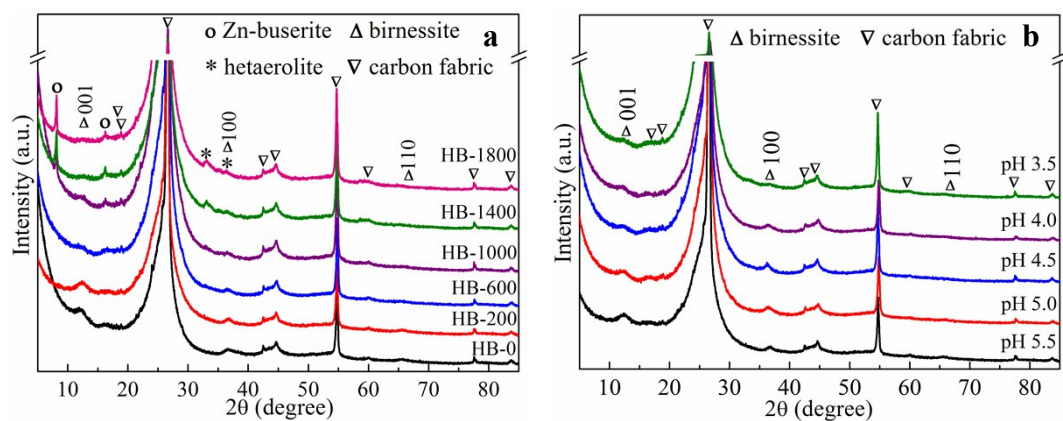


**Fig. S8** XRD patterns of birnessite electrodes after 50 cycles of charge–discharge tests in electrolyte with different concentrations of  $\text{Zn}^{2+}$  (a) and different pHs (b).

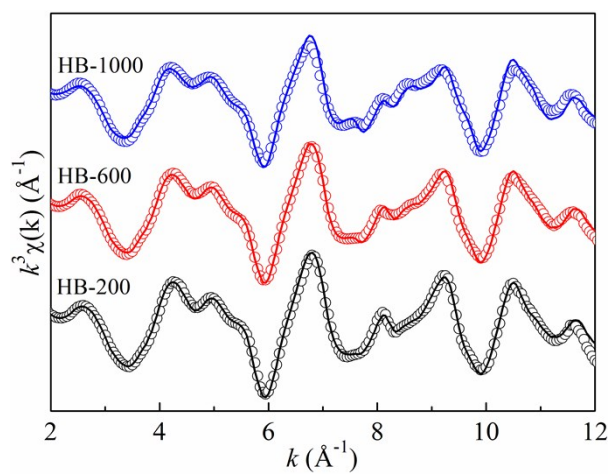


**Fig. S9** Mn K-edge  $k^3$ -weighted EXAFS spectra of birnessite electrodes after 50 cycles of charge–discharge tests in electrolytes with different  $\text{Zn}^{2+}$  concentrations (The lines are experimental curves and the dash dots are the best-fit linear combination).

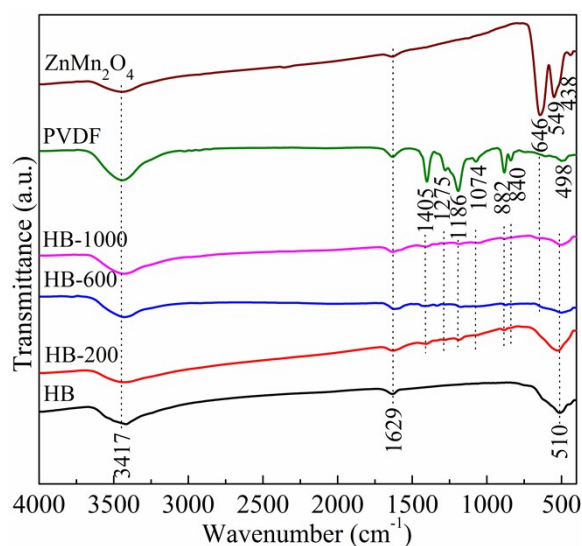


**Fig. S10** FTIR spectra of birnessite electrodes after 50 cycles of charge–discharge tests in electrolytes with different  $\text{Zn}^{2+}$  concentrations.

As seen from Fig. S10, the absorption bands at 3417 and 1629  $\text{cm}^{-1}$  could be attributed to the stretching and bending vibrations of crystal water and adsorbed water, respectively.<sup>5</sup> The band at 510  $\text{cm}^{-1}$  is due to the Mn–O stretching modes in the birnessite structure.<sup>5,6</sup> The bands at 646, 549 and 438  $\text{cm}^{-1}$  are ascribed the Mn–O vibration modes in  $\text{ZnMn}_2\text{O}_4$ .<sup>7</sup> The bands at 1405, 1275, 1186, 1074, 882, 840 and 498  $\text{cm}^{-1}$  are related to PVDF, which is consistent with previous report.<sup>8</sup> There was no peak of asymmetric stretching vibrations of  $\text{CO}_3^{2-}$  group at about 1515 and 1385  $\text{cm}^{-1}$ .<sup>9</sup> The above results further suggest that hydrozincite is not formed on birnessite electrode during the charge–discharge processes.

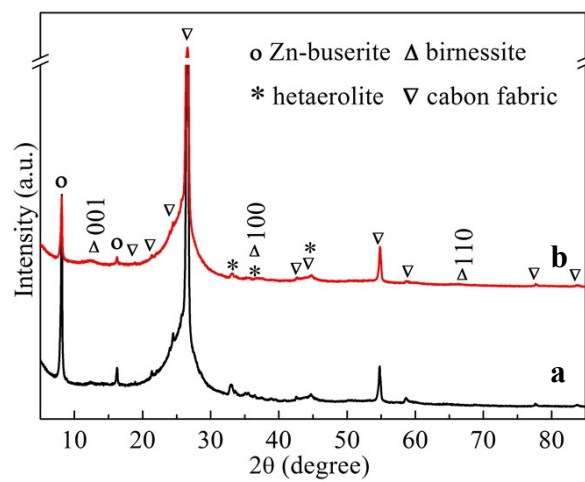


**Fig. S11** XRD patterns of birnessite electrodes after the first discharge (a) and the first charge–discharge (b) in  $0.1 \text{ mol L}^{-1} \text{ Na}_2\text{SO}_4$  electrolyte with  $1000 \text{ mg L}^{-1} \text{ Zn}^{2+}$ .

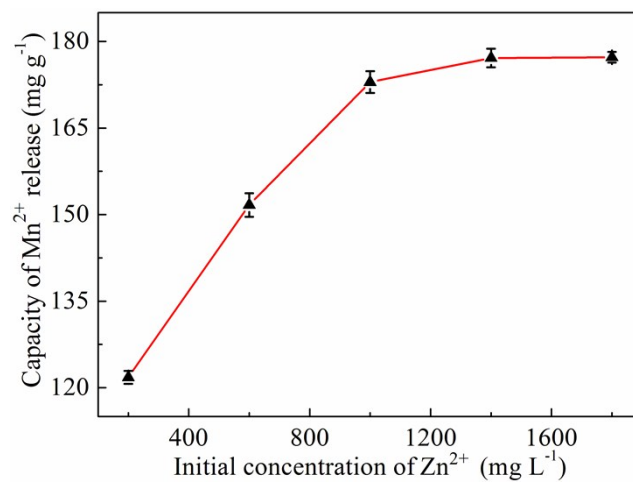


**Fig. S12** Mn<sup>2+</sup> release of birnessite electrode after 50 cycles of charge–discharge tests in electrolytes with different Zn<sup>2+</sup> concentrations.

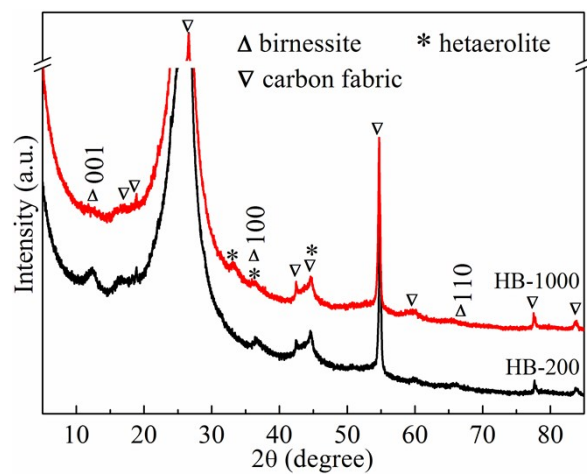


**Fig. S13** XRD patterns of HB-200 and HB-1000 electrodes after 50 cycles of charge–discharge tests in  $0.1 \text{ mol L}^{-1} \text{ Na}_2\text{SO}_4$  electrolyte.

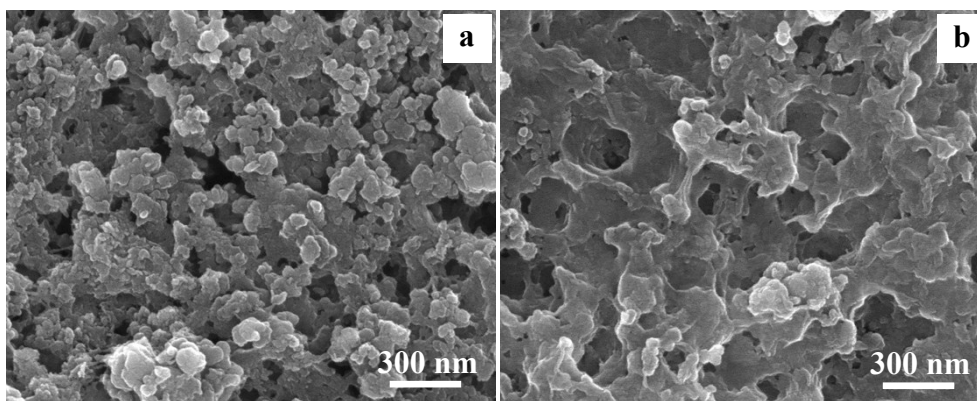


**Fig. S14** FESEM images of HB-200 (a) and HB-1000 (b) electrodes after 50 cycles of charge–discharge of tests in  $0.1 \text{ mol L}^{-1} \text{ Na}_2\text{SO}_4$  electrolyte.

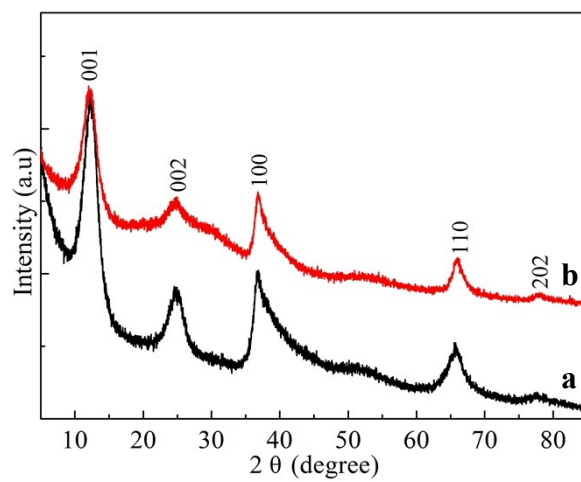


**Fig. S15** XRD patterns of pristine birnessite (a) and birnessite after isothermal adsorption experiment at Zn<sup>2+</sup> initial concentration of 650 mg L<sup>-1</sup> (b).

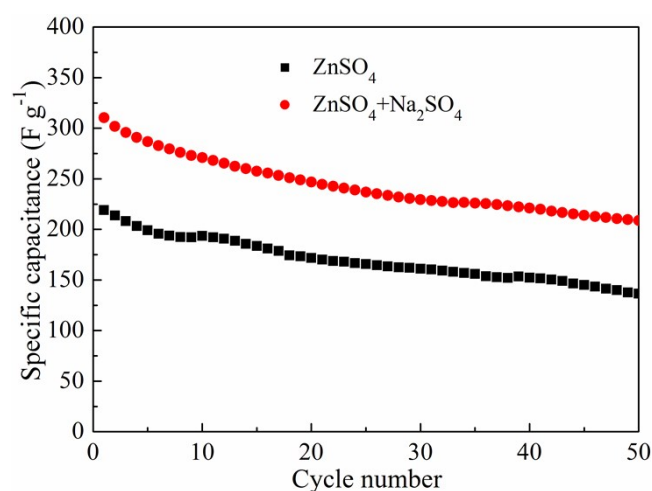


**Fig. S16** Cyclic capacitance of birnessite electrode at a current density of  $0.1 \text{ A g}^{-1}$  in  $200 \text{ mg L}^{-1}$   $\text{Zn}^{2+}$  electrolyte with/without  $\text{Na}_2\text{SO}_4$ .

## References

- 1 L. F. Xiao, Y. Y. Yang, J. Yin, Q. Li and L. Z. Zhang, *J. Power Sources*, 2009, **194**, 1089–1093.
- 2 H. S. Choi, S. J. Kim and J. J. Kim, *Geosci. J.*, 2004, **8**, 273–279.
- 3 L. H. Liu, M. Min, F. Liu, H. Yin, Y. S. Zhang and G. H. Qiu, *J. Power Sources*, 2015, **277**, 26–35.
- 4 A. Manceau, M. A. Marcus and S. Grangeon, *Am. Mineral.*, 2012, **97**, 816–827.
- 5 M. Huang, Y. X. Zhang, F. Li, L. L. Zhang, R. S. Ruoff, Z. Y. Wen and Q. Liu, *Sci. Rep.*, 2014, **4**, 3878.
- 6 X. J. Yang, Y. Makita, Z. H. Liu, K. Sakane and K. Ooi, *Chem. Mater.*, 2004, **16**, 5581–5588.
- 7 P. Zhang, X. Y. Li, Q. D. Zhao and S. M. Liu, *Nanoscale Res. Lett.*, 2011, **6**, 323.
- 8 Y. Peng and P. Y. Wu, *Polymer*, 2004, **45**, 5295–5299.
- 9 E. Turianicová, M. Kaňuchová, A. Zorkovská, M. Holub, Z. Bujňáková, E. Dutková, M. Baláž, L. Findoráková, M. Balintová and A. Obut, *J. CO<sub>2</sub> Util.*, 2016, **16**, 328–335.